Theor Chem Acc (2014) 133:1451
DOI 10.1007/s00214-014-1451-3

REGULAR ARTICLE

Properties of local vibrational modes: the infrared intensity

Wenli Zou · Dieter Cremer

Received: 12 September 2013 / Accepted: 13 January 2014 / Published online: 1 February 2014

Abstract For the local (adiabatic) vibrational modes of Konkoli and Cremer (Int J Quantum Chem 67:29–40, 1998), infrared intensities are derived by setting up the appropriate adiabatic conditions. It is shown that the local mode intensities are independent of the coordinates used to describe a molecule and correctly reflect the molecular symmetry and isotope composition. Normal mode intensities are related to local mode intensities via an adiabatic connection scheme (ACS). The ACS reveals intensity changes due to local mode mixing and avoided crossings, which are easily identified and quantified. The infrared intensities of simple molecules such as H_2O, CH_4, O_3, HOOH, CH_3OH, and the water dimer are discussed, and the influence of isotopes is quantified.

Keywords Local vibrational modes · Local stretching force constant · Infrared intensities · Local mode intensities · Adiabatic connection scheme · Isotope effects

1 Introduction

One of the primary objectives in chemistry is to determine the properties of the chemical bond [1]. Chemists have collected bond dissociation energies (BDE), bond lengths, stretching force constants, and other properties to derive suitable bond strength descriptors [2–4]. Although BDE values may be useful in a qualitative sense, they fail to be bond strength descriptors in a quantitative way because they depend on both the strength of the bond to be broken and the stabilization of the dissociation fragments caused by electron density redistribution, geometry relaxation, and avoided crossings between electronic states [5, 6]. The bond length has been used as bond strength descriptor for small, nonpolar molecules however becomes problematic for molecules with strongly polar bonds as is documented in the literature [7]. More suitable as bond strength descriptors are the stretching force constants of a vibrating molecule, which are obtained with the help of vibrational spectroscopy [4, 8, 9].

The use of stretching force constants to describe the chemical bond dates back to the 20s and 30s of the last century when Badger [10] found a relationship between force constant and bond length for diatomic molecules [11]. The extension of the Badger relationship to polyatomic molecules turned out to be difficult because spectroscopically derived stretching force constants are not unique, reflect coupling between the vibrational modes, and depend on the internal coordinates used for the description of the molecule in question [11]. Repeated attempts have been made to use stretching force constants by assuming that the bond stretching frequencies of certain functional groups are less effected by mode–mode coupling and therefore provide at least approximate measures for the bond strength via the associated force constants [12, 13]. These attempts are based on the general understanding that the stretching force constants of a molecule in its equilibrium geometry are the appropriate measures of the bond strength. Vibrational force constants are related to the curvature of the Born–Oppenheimer potential energy surface (PES) $E(\mathbf{q})$ spanned by the internal coordinates q_n of

Dedicated to Professor Thom Dunning and published as part of the special collection of articles celebrating his career upon his retirement.

W. Zou · D. Cremer (✉)
Computational and Theoretical Chemistry Group (CATCO), Department of Chemistry, Southern Methodist University, 3215 Daniel Ave, Dallas, TX 75275-0314, USA
e-mail: dieter.cremer@gmail.com; dcremer@gmail.com

the molecule in question. They can be obtained by calculating the Hessian of E(**q**), which collects all second derivatives of the molecular energy with regard to the q_n-coordinates and is identical (apart from some conversion factors) to the force constants matrix $\mathbf{F}^q$ expressed in terms of internal coordinates.

The stretching force constant corresponds to an infinitesimally small change of the bond, and therefore, it is an ideal dynamic measure of the bond strength, which is no longer influenced by electronic structure reorganization or geometry relaxation effects. However, the stretching force constants obtained for a polyatomic molecule by either directly calculating the Hessian matrix or, alternatively, deriving them from measured stretching frequencies by solving the basic equation of vibrational spectroscopy [8] can because of coupling effects, no longer be related to individual bonds. Therefore, vibrational spectroscopists have pursued various ways of obtaining local mode stretching force constants.

Already in the 60s, Decius [14] suggested to solve the force constant problem by reverting to the inverse force constant matrix $\mathbf{\Gamma} = (\mathbf{F}^q)^{-1}$ and introducing the compliance constants Γ_{nn} as local bond strength descriptors. Ample work has been carried out with the compliance constants to describe the properties of chemical bonds [15–19] although their physical meaning and relationship to the normal vibrational modes remained unclear. McKean [20–22] solved the problem of obtaining local XH stretching force constants by synthesizing isotopomers of a given molecule where all H atoms but the target hydrogen were replaced by deuterium. By measuring then the *isolated* XH stretching frequency, a reasonable approximation for a local mode frequency was obtained. Henry [23] obtained local mode information on CH-stretching vibrations from overtone spectra. Apart from this, there were numerous attempts to set up relationships between stretching force constants or frequencies and bond strength descriptors such as BDE values, bond orders, bond lengths, etc., which are discussed in a 2010 review article that underlines the necessity of obtaining local mode information from normal vibrational modes [11].

Konkoli and Cremer [24] determined for the first time local vibrational modes directly from normal vibrational modes by solving the mass-decoupled Euler–Lagrange equations. Each local mode is associated with an internal coordinate q_n ($n = 1,\ldots,N_{\text{vib}}$ with $N_{\text{vib}} = 3N - \Sigma$; N number of atoms; Σ number of translations and rotations), which drives the local mode [24]. These authors also demonstrated that each normal vibrational mode can be characterized in terms of local vibrational modes, where their characterization of normal mode (CNM) method is superior to the potential energy distribution analysis [11, 25]. Cremer et al. [26] developed a way of calculating from a complete set of $3N - \Sigma$ measured fundamental frequencies the corresponding local mode frequencies. In this way, one can distinguish between calculated harmonic local mode frequencies (force constants) and experimentally based local mode frequencies (force constants), which differ by anharmonicity effects [27, 28]. Larsson and Cremer [29] showed that McKean's isolated stretching frequencies are equal to the local mode frequencies if there is a complete decoupling of the CH-stretching modes in a deuterium isotopomer. Zou et al. [30] proved that the reciprocal of the compliance constant of Decius is identical with the local force constant of Konkoli and Cremer. Furthermore, they proved that the local vibrational modes of Konkoli and Cremer are the only modes, which directly relate to the normal vibrational modes.

A local mode depends only on the internal coordinate it is associated with (*leading parameter principle* [24]) and is independent of all other internal coordinates used to describe the geometry of a molecule. Accordingly, it is also independent of using redundant or non-redundant coordinate sets. The number of local vibrational modes can be larger than N_{vib}, and therefore, it is important to determine those local modes, which are essential for the reproduction of the normal modes. They can be determined with the help of an adiabatic connection scheme (ACS), which relates local vibrational frequencies to normal vibrational frequencies by increasing a scaling factor λ from 0 (local frequencies) to 1 (normal frequencies). For a set of redundant internal coordinates and their associated local modes, all those frequencies converge to zero for $\lambda \rightarrow 1$, which do not contribute to the normal modes so that a set of N_{vib} dominant local modes remains [30, 31].

The infrared intensities of vibrational modes have been used to determine effective atomic charges of a molecule [32–34]. The measured intensities are associated with the atomic polar tensor (APT), which is the matrix of dipole moment derivatives with regard to the geometrical parameters of a molecule. If it is possible to obtain the APT from measured infrared intensities and if in addition the geometry of a molecule is known, one can directly determine effective atomic charges from measured infrared intensities. Much work has been done in this direction [32–35] where however all attempts so far have been based on normal rather than local vibrational modes. Since each normal mode is delocalized because of mode–mode coupling, it is questionable whether reliable charge information can be obtained from normal mode intensities. It is much more likely that in these cases, as in the case of the bond strength description, local mode rather than normal mode information is needed.

In this work, we will make the first and necessary step for obtaining effective atomic and bond charges from infrared intensities and APT by deriving the local mode intensity. Furthermore, we will relate the local mode intensities to those of the normal modes utilizing an intensity ACS as was recently done for the frequency ACS [30]. Equipped with these theoretical tools, we will be able to analyze normal mode intensities and discuss them in terms of local mode intensities, mode–mode coupling, isotope-dependence, and symmetry.

Before doing so it is necessary to clarify the term *local mode* because it is used in the literature in at least four different ways. (i) In computational chemistry, the normal modes are calculated using the classical description of a vibrating molecule introduced by Wilson et al. [8]. In this description, normal modes are delocalized because of mode coupling and their counterparts (derived by Konkoli and Cremer [24]) are the *local modes* of this work. Other terms such as *isolated* [20] or *intrinsic* [36] have been used in connection with local mode descriptions, but these latter terms refer to normal vibrational modes, which are *local* only in an approximate sense. (ii) Henry et al. [23, 37–40] have developed local mode (an)harmonic oscillator models to quantum mechanically calculate the overtones of XH stretching modes. The higher overtone modes ($n = 5$ or 6) for isolated XH groups are largely decoupled, which justifies speaking of local modes. Contrary to the normal and local modes of classical physics (see i), the local modes of the oscillator models and their frequencies are true eigenfunctions and eigenvalues of a quantum mechanical Hamiltonian acting on the vibrational wave function. (iii) Reiher et al. [41–43] calculate unitarily transformed normal modes associated with a given band in the vibrational spectrum of a polymer where the criteria for the transformation are inspired by those applied for the localization of molecular orbitals. The authors speak in this case of local vibrational modes because the modes are localized in just a few units of a polymer. Nevertheless, Reihers local modes are still delocalized within the polymer units. (iv) Yet, another use of the term local modes is made in solid-state physics where it refers to the vibrational mode(s) of an impurity in a solid material [44, 45].

The results of this work will be presented in three sections. In Sect. 2, the theory of the local mode intensities and the intensity ACS will be developed. Local mode intensities are analyzed and discussed for some small molecules in Sect. 3. It is shown how the normal mode intensities can be stepwise converted into local mode intensities and vice versa. In Sect. 4, the chemical relevance of the local mode intensities is discussed. In the final section, conclusions are drawn and an outlook is presented.

2 Theory of local vibrational modes

The vibrational secular equation expressed in Cartesian coordinates is given by Eq. (1): [8, 9, 46]

$$\mathbf{F}^x\tilde{\mathbf{L}} = \mathbf{M}\tilde{\mathbf{L}}\mathbf{\Lambda} \tag{1}$$

where $\mathbf{F}^x$ is the force constant matrix, $\mathbf{M}$ the mass matrix, matrix $\tilde{\mathbf{L}}$ collects the vibrational eigenvectors $\tilde{\mathbf{l}}_\mu$ in its columns, and $\mathbf{\Lambda}$ is a diagonal matrix with the eigenvalues λ_μ, which leads to the (harmonic) vibrational frequencies ω_μ according to $\lambda_\mu = 4\pi^2c^2\omega_\mu^2$. In Eq. (1), the number of vibrational modes is given by N_{vib}, i.e., Σ translational and rotational motions of the molecule are already eliminated. Here and in the following, a tilde above a vector or matrix symbol indicates mass weighting. Matrix $\tilde{\mathbf{L}}$ has the following properties

$$\tilde{\mathbf{L}}^\dagger\mathbf{M}\tilde{\mathbf{L}} = \mathbf{I} \tag{2}$$

$$\tilde{\mathbf{L}}^\dagger\mathbf{F}^x\tilde{\mathbf{L}} = \mathbf{\Lambda} \tag{3}$$

i.e., matrix $\tilde{\mathbf{L}}$ and eigenvalue matrix $\mathbf{\Lambda}$ are obtained by diagonalization of the mass-weighted force constant matrix. Usually, the normal mode vectors $\tilde{\mathbf{l}}_\mu$ are re-normalized according to

$$\mathbf{l}_\mu = \frac{1}{\sqrt{\tilde{\mathbf{l}}_\mu^\dagger\tilde{\mathbf{l}}_\mu}}\tilde{\mathbf{l}}_\mu = \sqrt{m_\mu^R}\tilde{\mathbf{l}}_\mu \tag{4}$$

or

$$\mathbf{L} = \tilde{\mathbf{L}}(\mathbf{M}^R)^{1/2} \tag{5}$$

where $m_\mu^R = \left(\tilde{\mathbf{l}}_\mu^\dagger\tilde{\mathbf{l}}_\mu\right)^{-1}$ is the reduced mass of mode μ.

Matrix $\mathbf{L}$ also satisfies Eq. (1) in the form

$$\mathbf{F}^x\mathbf{L} = \mathbf{M}\mathbf{L}\mathbf{\Lambda} \tag{6}$$

which leads to

$$\mathbf{L}^\dagger\mathbf{F}^x\mathbf{L} = \mathbf{K} \tag{7}$$

$$\mathbf{L}^\dagger\mathbf{M}\mathbf{L} = \mathbf{M}^R \tag{8}$$

Equations (7) and (8) define the diagonal normal force constant matrix $\mathbf{K}$ and the reduced mass matrix $\mathbf{M}^R$ (with elements m_μ^R), respectively.

The vibrational secular equation expressed in internal coordinates q_n is given by Wilson et al. [8]

$$\mathbf{F}^q\tilde{\mathbf{D}} = \mathbf{G}^{-1}\tilde{\mathbf{D}}\mathbf{\Lambda} \tag{9}$$

Here, $\tilde{\mathbf{D}}$ contains the normal mode vectors $\tilde{\mathbf{d}}_\mu(\mu = 1, \ldots, N_{vib})$, and matrix $\mathbf{G} = \mathbf{B}\mathbf{M}^{-1}\mathbf{B}^\dagger$ (Wilson matrix) gives the kinetic energy in terms of internal coordinates [8]. The eigenvector matrix $\tilde{\mathbf{D}}$ has the properties

$$\tilde{\mathbf{D}}^{\dagger}\mathbf{G}^{-1}\tilde{\mathbf{D}} = \mathbf{I} \tag{10}$$

$$\tilde{\mathbf{D}}^{\dagger}\mathbf{F}^{q}\tilde{\mathbf{D}} = \mathbf{\Lambda} \tag{11}$$

Renormalization of $\tilde{\mathbf{D}}$ according to

$$\mathbf{D} = \tilde{\mathbf{D}}(\mathbf{M}^{R})^{1/2} \tag{12}$$

leads to

$$\mathbf{F}^{q}\mathbf{D} = \mathbf{G}^{-1}\mathbf{D}\mathbf{\Lambda} \tag{13}$$

and

$$\mathbf{D}^{\dagger}\mathbf{F}^{q}\mathbf{D} = \mathbf{K} \tag{14}$$

$$\mathbf{D}^{\dagger}\mathbf{G}^{-1}\mathbf{D} = \mathbf{M}^{R} \tag{15}$$

The relationship between $\mathbf{D}(\tilde{\mathbf{D}})$ and $\mathbf{L}(\tilde{\mathbf{L}})$ is given by Zou et al. [31]

$$\mathbf{L} = \mathbf{C}\mathbf{D} \tag{16}$$

$$\tilde{\mathbf{L}} = \mathbf{C}\tilde{\mathbf{D}} \tag{17}$$

Matrix $\mathbf{C}$ is the pseudo-inverse matrix of $\mathbf{B}$, where the latter is a rectangular ($N_{\text{vib}} \times 3N$) matrix containing the first derivatives of the internal coordinates q_n with regard to the Cartesian coordinates.

$$\mathbf{C} = \mathbf{M}^{-1}\mathbf{B}^{\dagger}\mathbf{G}^{-1} \tag{18}$$

Equations (1)–(18) are needed to present and derive in the following the properties of the local vibrational modes.

2.1 Properties of a local mode

The local vibrational modes of Konkoli and Cremer [24] can be directly determined from the normal vibrational modes. The local mode vector $\mathbf{a}_n$ associated with $q_n (n = 1, \ldots, N_{\text{para}}$ with N_{para} being the number of internal coordinates to specify the molecular geometry) is given by

$$\mathbf{a}_n = \frac{\mathbf{K}^{-1}\mathbf{d}_n^{\dagger}}{\mathbf{d}_n\mathbf{K}^{-1}\mathbf{d}_n^{\dagger}} \tag{19}$$

where the local mode is expressed in terms of normal coordinates Q_μ associated with force constant matrix $\mathbf{K}$. Here, $\mathbf{d}_n$ denotes a row vector of the matrix $\mathbf{D}$. The local mode force constant k_n^a of mode n (superscript a denotes an adiabatically relaxed, i.e., local mode) is obtained with Eq. (20):

$$k_n^a = \mathbf{a}_n^{\dagger}\mathbf{K}\mathbf{a}_n = (\mathbf{d}_n\mathbf{K}^{-1}\mathbf{d}_n^{\dagger})^{-1} \tag{20}$$

Local mode force constants, contrary to normal mode force constants, have the advantage of being independent of the choice of the coordinates to describe the molecule in question [24, 26]. In recent work, Zou et al. [30, 31] proved that the compliance constants Γ_{nn} of Decius [14] are simply the reciprocal of the local mode force constants: $k_n^a = 1/\Gamma_{nn}$.

The reduced mass of the local mode $\mathbf{a}_n$ is given by the reciprocal diagonal element G_{nn} of the $\mathbf{G}$-matrix [24]. Local mode force constant and mass are sufficient to determine the local mode frequency ω_n^a

$$(\omega_n^a)^2 = \frac{1}{4\pi^2 c^2} k_n^a G_{nn} \tag{21}$$

2.2 Adiabatic connection scheme (ACS) relating local to normal mode frequencies

With the help of the compliance matrix $\mathbf{\Gamma}^q = (\mathbf{F}^q)^{-1}$, the vibrational eigenvalue Eq. (9) can be expressed as [30]

$$(\mathbf{\Gamma}^q)^{-1}\tilde{\mathbf{D}} = \mathbf{G}^{-1}\tilde{\mathbf{D}}\mathbf{\Lambda} \tag{22}$$

or

$$\mathbf{G}\tilde{\mathbf{R}} = \mathbf{\Gamma}^q\tilde{\mathbf{R}}\mathbf{\Lambda} \tag{23}$$

where a new eigenvector matrix $\tilde{\mathbf{R}}$ is given by

$$\tilde{\mathbf{R}} = (\mathbf{\Gamma}^q)^{-1}\tilde{\mathbf{D}} = \mathbf{F}^q\tilde{\mathbf{D}} = (\tilde{\mathbf{D}}^{-1})^{\dagger}\mathbf{K} \tag{24}$$

Next, the matrices $\mathbf{\Gamma}^q$ and $\mathbf{G}$ are partitioned into diagonal ($\mathbf{\Gamma}_d^q$ and $\mathbf{G}_{\text{d}}$) and off-diagonal ($\mathbf{\Gamma}_{od}^q$ and $\mathbf{G}_{\text{od}}$) parts: [30]

$$(\mathbf{G}_d + \lambda\mathbf{G}_{od})\tilde{\mathbf{R}}_\lambda = (\mathbf{\Gamma}_d^q + \lambda\mathbf{\Gamma}_{od}^q)\tilde{\mathbf{R}}_\lambda\mathbf{\Lambda}_\lambda \tag{25}$$

where the off-diagonal parts can be successively switched on with a scaling factor λ ($0 \le \lambda \le 1$), so that the local mode description given by the diagonal parts ($\lambda = 0$) is stepwise converted into the normal mode description obtained for $\lambda = 1$. For each value of λ a specific set of eigenvectors and eigenvalues collected in $\tilde{\mathbf{R}}_\lambda$ and $\mathbf{\Lambda}_\lambda$, respectively, is obtained. Equation (25) is the basis for the ACS.

2.3 Infrared intensity of a normal mode

The infrared intensity of normal mode μ is determined by [34, 47, 48]

$$I_\mu^{nm} = (\boldsymbol{\delta}_\mu^{nm})^{\dagger}\boldsymbol{\delta}_\mu^{nm} \tag{26}$$

where superscript nm denotes a normal mode and the dipole derivative vectors $\boldsymbol{\delta}_\mu^{nm}$ are collected in a matrix $\boldsymbol{\delta}^{nm}$ given by Eq. (27):

$$\boldsymbol{\delta}^{nm} = \mathscr{C}\mathbf{\Delta}\tilde{\mathbf{L}} = \mathscr{C}\mathbf{\Delta}\mathbf{L}(\mathbf{M}^{R})^{-1/2} \tag{27}$$

The APT matrix $\mathbf{\Delta}$ is of dimension $3 \times 3N$ and contains the dipole moment derivatives with regard to Cartesian coordinates [32, 34]. If the normal mode intensity I_μ^{nm} is

given in km/mol and $\mathbf{\Lambda}$ and $\mathbf{M}^R$ in atomic units, the conversion factor $\mathscr{C}$ in Eq. (27) is 31.22307.

2.4 Infrared intensity of a local mode

The intensity I_n^a of a local mode $\mathbf{a}_n$ associated with internal coordinate q_n has to fulfill a number of requirements: (i) I_n^a must be characteristic of the local mode in question (and the associated displacement coordinate), however independent of any other internal coordinate used for the description of the molecular geometry. (ii) It must be characteristic of the masses of the atoms participating in the local vibration, but at the same time it must be independent of any other atomic masses in the molecule. (iii) In case of symmetry, symmetry-equivalent local modes must possess identical intensities. (iv) For diatomic molecules, the local mode intensity must be identical with the normal mode intensity.

For the derivation of the local mode intensity, Eq. (27) is re-written in terms of internal coordinates utilizing Eqs. (10), (17), and (18):

$$\boldsymbol{\delta}^{nm} = \mathscr{C}\mathbf{\Lambda}\left(\mathbf{M}^{-1}\mathbf{B}^{\dagger}\mathbf{G}^{-1}\right)\tilde{\mathbf{D}} \tag{28}$$

$$= \mathscr{C}\mathbf{\Lambda}\mathbf{M}^{-1}\mathbf{B}^{\dagger}(\tilde{\mathbf{D}}^{\dagger})^{-1} \tag{29}$$

If $N_{\text{para}} = N_{\text{vib}}$, the inverse of $\tilde{\mathbf{D}}$ exists.

For the adiabatic situation with $\lambda = 0$, Eq. (22) becomes

$$(\mathbf{\Gamma}^q)_d^{-1}\tilde{\mathbf{D}}_0 = \mathbf{G}_d^{-1}\tilde{\mathbf{D}}_0\mathbf{\Lambda} \tag{30}$$

and the normalization condition (10) takes the form

$$\tilde{\mathbf{D}}_0^{\dagger}\mathbf{G}_d^{-1}\tilde{\mathbf{D}}_0 = \mathbf{I} \tag{31}$$

where the subscript 0 denotes $\lambda = 0$. If the local modes are ordered according to increasing frequencies ω_μ^2, then matrix $\tilde{\mathbf{D}_0}$ will be diagonal. Hence, matrix $\mathbf{D}_0 = \mathbf{G}_d^{-1/2}\tilde{\mathbf{D}_0}$ is also diagonal where $\mathbf{M}_0^R = \mathbf{G}_d^{-1}$. Accordingly, it holds that

$$\mathbf{D}_0^{\dagger}\mathbf{D}_0 = \tilde{\mathbf{D}}_0^{\dagger}\mathbf{G}_d^{-1}\tilde{\mathbf{D}}_0 = \mathbf{I} \tag{32}$$

or

$$\sum_{\nu}^{N_{\text{vib}}}(\mathbf{D}_0)_{\mu\nu}(\mathbf{D}_0)_{\nu\mu} = (\mathbf{D}_0)_{\mu\mu}^2 = 1 \tag{33}$$

which implies that $(\mathbf{D}_0)_{\mu\mu} = \pm 1$ where only the positive value is used for reasons of simplicity. We conclude that matrix $\mathbf{D}_0$ is the unit matrix.

Hence, the local mode condition with $\lambda = 0$ implies that (i) $\mathbf{D}_0 = \mathbf{I}$, (ii) $\mathbf{M}_0^R = \mathbf{G}_d^{-1}$, and (iii) $\tilde{\mathbf{D}}_0 = \mathbf{G}_d^{1/2}$. Equation (29) takes for local mode $\mathbf{a}_n$ the form

$$\boldsymbol{\delta}^a = \mathscr{C}\mathbf{\Lambda}\mathbf{M}^{-1}\mathbf{B}^{\dagger}\mathbf{G}_d^{-1/2} \tag{34}$$

which leads to the local mode intensity

Table 1 Local and normal mode intensities I_n^a and I_μ^{nm} of H_2O and HDO

Molecule	Parameter	I_n^a (km/mol)	Mode μ	I_μ^{nm} (km/mol)
H_2O	H–O	23.4868	1	40.8595
	H–O	23.4868	2	3.2361
	H–O–H	69.1712	3	69.5078
	H·H	11.3848		
HDO	H–O	23.4868	1	24.7171
	D–O	14.9527	2	11.2932
	H–O–D	59.8634	3	59.5745
	D–O	14.9527		
	H·D	16.9479		

B3LYP/cc–pVTZ calculations based on Eqs. (26) and (34)

$$I_n^a = (\boldsymbol{\delta}_n^a)^{\dagger}\boldsymbol{\delta}_n^a \tag{35}$$

It can be easily proved that Eq. (34) is both isotope-independent and parameter-independent and, in addition, leads to symmetry-equivalent intensities thus fulfilling the requirements (i), (ii), and (iii) for local mode intensities. For a diatomic molecule, Eq. (34) collapses to Eq. (27). The fulfillment of (i), (ii), and (iii) is demonstrated for the water molecule (see Table 1).

The water example shows that the bending intensity is relatively large and literally identical for normal and local mode where the difference results from a small coupling between bending and symmetric stretching mode. The local OH stretching intensities are identical and of medium size, which changes as a consequence of coupling between the two OH stretching modes. The symmetric stretching mode has only a small intensity because it leads to a relatively small change in the charge distribution. It is noteworthy that the measured intensity of the symmetric stretching mode is 2.2 km/mol [33], which is a result of a small mixing of stretching and bending vibration. The asymmetric stretching mode causes a large change in the charge distribution and accordingly has a large normal mode intensity.

If the bending parameter is replaced by the distance between the H atoms, a much lower intensity is obtained because the charge changes become smaller during this non-bonded stretching motion. However, none of the OH stretching vibrations changes its intensity value confirming that the local modes are independent of the other internal coordinates used for determining the molecular geometry. In this connection, it is important to note that the HH distance is used here only for test purposes. If the frequency ACS of the water molecule is set up with a redundant set of six internal coordinates (three distances and three angles in a hypothetical triangle), three local

mode frequencies associated with HH distance and the two OHH angles converge to zero.

If one H is replaced by D, the local DO stretching intensity adopts a lower value because of the large mass of the D atom. Again, this does not lead to a change in the local OH stretching intensity. Also, there is no change when the bending angle is replaced by the H · D non-bonded distance.

Because of the parameter-independence, Eq. (34) can be formulated for an individual local mode associated with q_n as

$$\boldsymbol{\delta}_n^a = \frac{\mathscr{C}}{\sqrt{G_{nn}}}\boldsymbol{\Delta}\mathbf{M}^{-1}\mathbf{b}_n^\dagger \tag{36}$$

where $\mathbf{b}_n$ is a vector of matrix $\mathbf{B}$. Since $\mathbf{b}_n^\dagger/\sqrt{G_{nn}}$ has the unit of amu$^{1/2}$, the conversion factor $\mathscr{C}$ in Eq. (36) does not depend on $\mathbf{b}_n$, i.e., the conversion factors for bond stretching, bending, or torsion are the same, which is different from the case of local mode force constants [31].

2.5 Adiabatic connection scheme for intensities

Equation (29) can be used as a starting point for deriving an ACS for infrared intensities.

$$\boldsymbol{\delta}_\lambda = \mathscr{C}\boldsymbol{\Delta}\mathbf{M}^{-1}\mathbf{B}^\dagger(\tilde{\mathbf{D}}_\lambda^\dagger)^{-1} \tag{37}$$

i.e., the intensity I_λ depends on the eigenvector matrix $\tilde{\mathbf{D}}_\lambda$ obtained from Eq. (38):

$$\boldsymbol{\Gamma}_\lambda^{-1}\tilde{\mathbf{D}}_\lambda = \mathbf{G}_\lambda^{-1}\tilde{\mathbf{D}}_\lambda\boldsymbol{\Lambda}_\lambda \tag{38}$$

or

$$\left(\boldsymbol{\Gamma}_d^q + \lambda\boldsymbol{\Gamma}_{od}^q\right)^{-1}\tilde{\mathbf{D}}_\lambda = (\mathbf{G}_d + \lambda\mathbf{G}_{od})^{-1}\tilde{\mathbf{D}}_\lambda\boldsymbol{\Lambda}_\lambda \tag{39}$$

with the scaling factor λ increasing from 0 (local modes; $\tilde{\mathbf{D}}_{\lambda=0} = \mathbf{G}_d^{1/2}$ and $\boldsymbol{\delta}_{\lambda=0} = \boldsymbol{\delta}^a$) to 1 (normal modes; $\tilde{\mathbf{D}}_{\lambda=1} = \tilde{\mathbf{D}}$ and $\boldsymbol{\delta}_{\lambda=1} = \boldsymbol{\delta}^{nm}$).

Equation (39) has a number of advantages compared with Eq. (25). The latter becomes unstable in the case of small normal mode frequencies associated with small normal mode force constants because $\tilde{\mathbf{R}}$ of Eq. (24) becomes also small. This can no longer happen if one works with the inverse of matrices $\mathbf{G}_\lambda$ and $\boldsymbol{\Gamma}_\lambda$.

In the following, we give some application examples, which illustrate the method described. Also, the usefulness of local mode intensities is discussed.

3 Local mode intensities and ACS for infrared intensities

In Figs. 1a–d, 2a, b and 3a, b, intensity and frequency ACS diagrams are shown for H_2O, CH_4, O_3, HOOH, CH_3OH, and the water dimer, $(H_2O)_2$, as obtained (if not otherwise noted) at the ωB97X-D/aug–cc–pVTZ level of theory [49, 50]. For ozone, CCSD/aug–cc–pVTZ calculations were carried out to get more reliable results. The calculated geometries and the notation of the atoms are given in Fig. 4. In Table 2, calculated normal and local mode frequencies and intensities are compared. In the following, we will discuss interesting features of the intensity ACS, which help to understand the magnitude of the normal mode intensity.

3.1 Water

The two local OH stretching modes are equivalent and, accordingly, the two local OH stretching frequencies are identical as are the corresponding intensities (see Fig. 1a). These identities reflect the symmetry of the molecule although none of the two local OH stretching vectors can by classified to have a symmetry of the C_{2v} point group. However, an infinitesimal increase of λ by ϵ leads to an large change in the OH stretching intensities caused by the fact that the symmetry of the molecule is switched on. In this sense, $\lambda = \varepsilon$ ($\varepsilon \to 0$) denotes a catastrophe point [51] in the ACS diagram for intensities (according to Thom's theory of catastrophes) [52].

Contrary to the vibrational frequencies, the λ-dependent intensities explicitly depend on the mode vectors [see Eq. (37)]. For a given normal mode μ, one can define the mode dependent part as

$$\mathbf{t}_\mu(\lambda) = [(\tilde{\mathbf{D}}_\lambda^\dagger)^{-1}]_\mu = [(\mathbf{G}_\lambda)^{-1}\tilde{\mathbf{D}}_\lambda]_\mu \tag{40}$$

which in the case of the local mode ($\lambda = 0$) becomes

$$\mathbf{t}_n(\lambda = 0) = [(\tilde{\mathbf{D}}_{\lambda=0}^\dagger)^{-1}]_n = [\mathbf{G}_d^{-1/2}]_n \tag{41}$$

i.e., the local mode vector $\mathbf{t}_n$ contains only zeroes with the exception of position n.

This may be demonstrated for H_2O at $\lambda = 0$ where the following matrix contains the three column vectors $\mathbf{t}_n$ corresponding to internal coordinates H–O–H, O–H1, and O–H2:

$$\begin{pmatrix} 0.0000 & 0.0000 & 0.9737 \\ 0.0000 & 0.9737 & 0.0000 \\ 1.2416 & 0.0000 & 0.0000 \end{pmatrix} \tag{42}$$

At $\lambda = \varepsilon = 10^{-4}$, the column vectors change strongly

$$\begin{pmatrix} -0.0001 & 0.6886 & 0.6885 \\ -0.0001 & 0.6886 & -0.6885 \\ 1.2416 & 0.0008 & 0.0000 \end{pmatrix} \tag{43}$$

indicating that there is an intensity catastrophe leading to the splitting into a large asymmetric OH stretching intensity and a small symmetric OH stretching intensity.

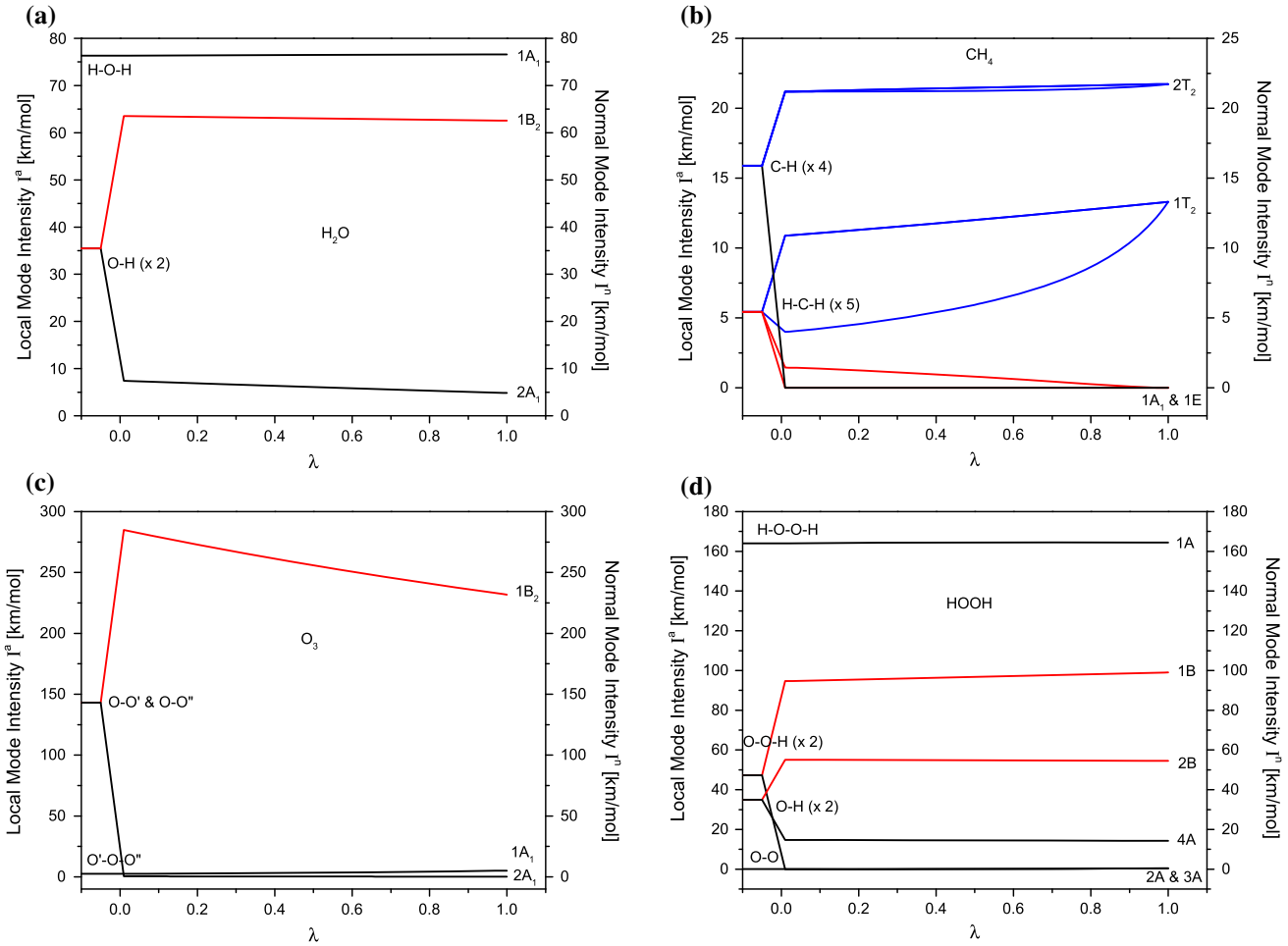

Fig. 1 Intensity ACS for **a** water, **b** methane, **c** ozone, and **d** hydrogen peroxide. The different mode symmetries are indicated by *different colors*. For the purpose of identifying intensity catastrophes, the $I(\lambda)$ curves are started with an arbitrary negative λ value so that the splitting at $\lambda = 0$ can be made visible. For the numbering of atoms, see Fig. 4. ωB97X-D/aug–cc–pVTZ or CCSD/aug–cc–VTZ (ozone) calculations

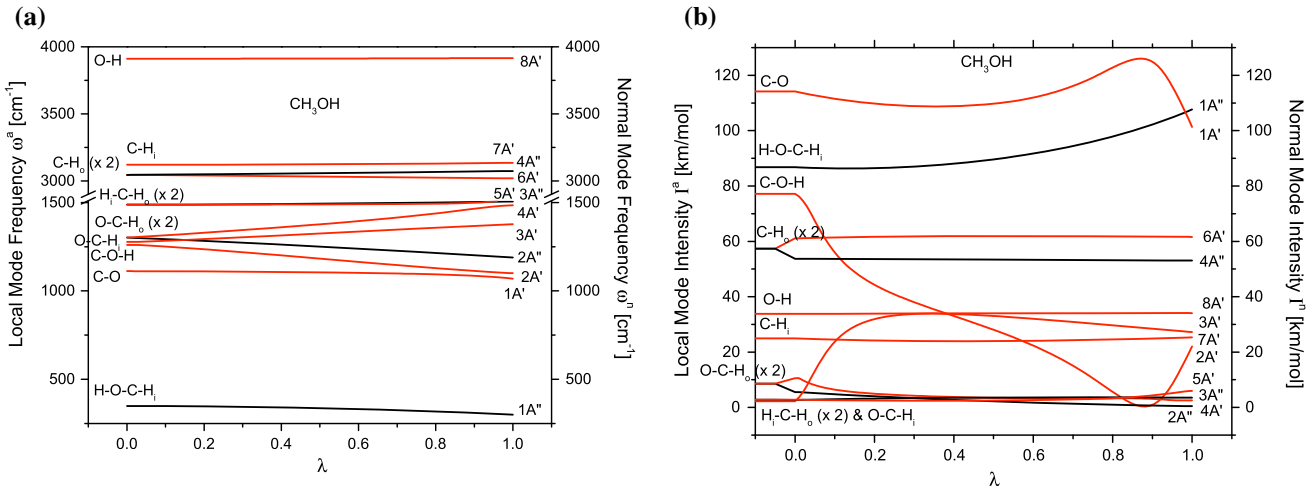

Fig. 2 **a** Frequency and **b** intensity ACS for methanol, CH_3OH. The different mode symmetries are indicated by *different colors*. For the purpose of identifying intensity catastrophes, the $I(\lambda)$ curves are started with an arbitrary negative λ value so that the splitting at $\lambda = 0$ can be made visible. For the numbering of atoms, see Fig. 4 . ωB97X-D/aug–cc–pVTZ calculations

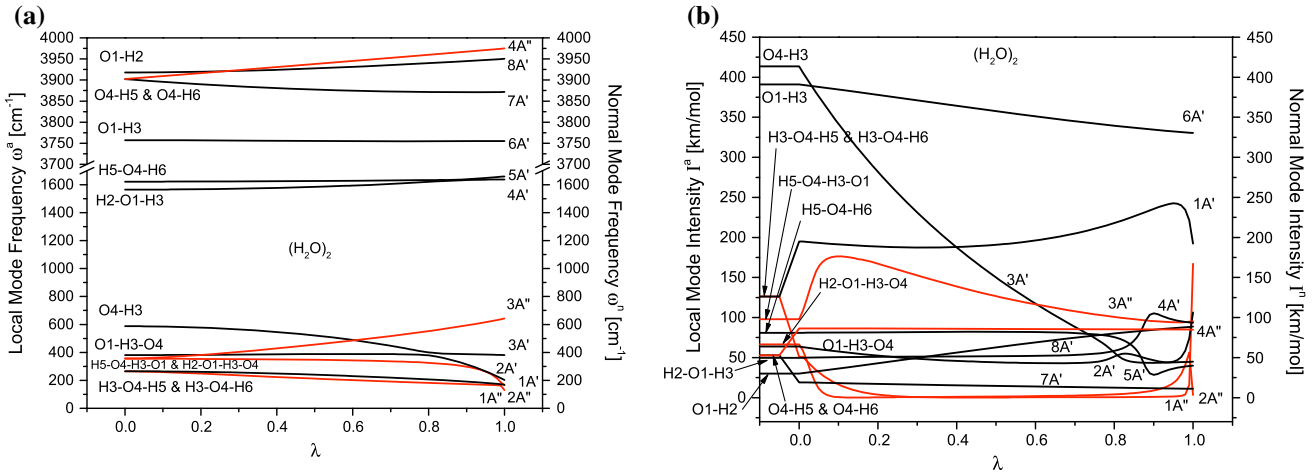

Fig. 3 **a** Frequency and **b** intensity ACS for the water dimer, $(H_2O)_2$. The different mode symmetries are indicated by *different colors*. For the purpose of identifying intensity catastrophes, the I (λ) curves are started with an arbitrary negative λ value so that the splitting at $\lambda = 0$ can be made visible. For the numbering of atoms, see Fig. 4. ωB97X-D/aug–cc–pVTZ calculations

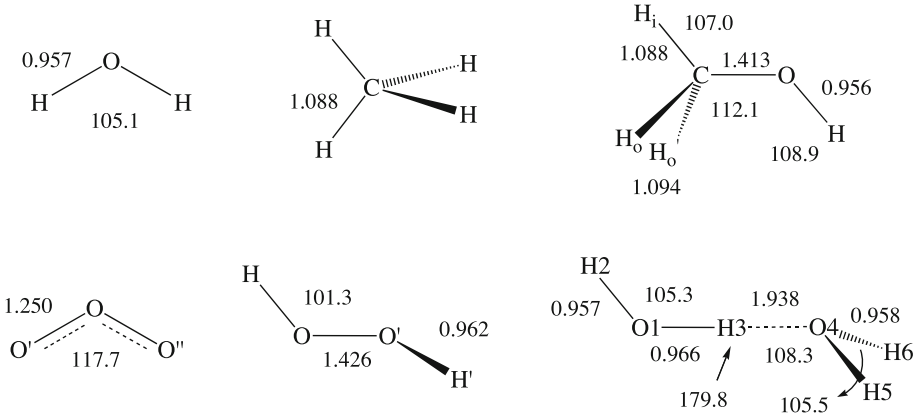

Fig. 4 ωB97X-D/aug–cc–pVTZ or CCSD/aug–cc–VTZ (ozone) geometries of the molecules investigated

The magnitude of the intensity splitting for equivalent modes depends on the corresponding values of the APT (the change in the charge distribution caused by the local mode), the ratio of the masses involved and the coupling of the mode vectors. In the case of H_2O, the two stretching mode vectors involve as a common atom the O atom, which is a prerequisite for a large coupling (proximity effect). However, the angle between the mode vectors is with 105° (Fig. 4) close to 90° where the coupling of the OH stretching modes vanishes. Also the light–heavy–light situation of the three atoms involved leads to a smaller coupling. However, the changes in the charge distribution upon OH stretching are significant so that the splitting values ΔI of the local OH stretching intensities at the catastrophe point takes a medium-seized value of ±28 km/mol (see Table 3; Fig. 1a).

An intensity catastrophe is not found in the case of isotopomer HOD because of the difference in the OH and OD stretching modes. At $\lambda = 0$, three different $\mathbf{t}_n$ vectors are determined:

$$\begin{pmatrix} 0.0000 & 0.0000 & 0.9737 \\ 0.0000 & 1.3375 & 0.0000 \\ 1.4164 & 0.0000 & 0.0000 \end{pmatrix} \tag{44}$$

and at $\lambda = \varepsilon$,

$$\begin{pmatrix} 0.0001 & 0.0007 & 0.9737 \\ 0.0001 & 1.3375 & -0.0007 \\ 1.4164 & 0.0008 & 0.0006 \end{pmatrix} \tag{45}$$

for which the changes are moderate in comparison to (44). It can be concluded that *sudden changes* in the intensity are connected with catastrophe points caused by a switching on of the molecular symmetry as a result of an infinitesimal change of $\lambda = 0$ to $\lambda = \varepsilon$.

3.2 Other examples with catastrophe points

CH_4, O_3, and HOOH. For methane, $N_{vib} = N_{para} = 9$ where the four CH bond lengths and five of the six H–C–H bending angles are used. There are just two local mode

Table 2 Comparison of normal mode and local mode frequencies and intensities obtained by ωB97X-D/aug–cc–pVTZ or CCSD/aug–cc–VTZ (ozone) calculations

Molecule mode μ	Sym.	ω_μ^{nm} (cm^{-1})	I_μ^{nm} (km/mol)	Local mode parameter n	ω_n^a (cm^{-1})	I_n^a (km/mol)
H_2O	C_{2v}					
1	A_1	1,634.8	76.6	HOH	1,634.8	76.4
2	A_1	3,878.3	4.9	OH	3,913.2	35.5
3	B_2	3,985.4	62.6	OH′	3,913.2	35.5
CH_4	T_d					
1, 2, 3	$1T_2$	1,360.4	13.3	HCH (×3)	1,450.1	5.4
4, 5	1E	1,577.0	0	HCH (×2)	1,450.1	5.4
6	$1A_1$	3,041.7	0	CH	3,126.2	15.9
7, 8, 9	$2T_2$	3,159.8	21.7	CH (×3)	3,126.2	15.9
O_3	C_{2v}					
1	$1A_1$	761.8	5.2	O′OO″	866.5	2.5
2	$1B_2$	1,253.7	231.8	OO′	1,249.7	143.0
3	$2A_1$	1,272.9	0.2	OO″	1,249.7	143.0
HOOH	C_2					
1	1A	3,93.5	164.5	HOO′H′	394.0	164.0
2	2A	1,025.6	0.4	OO′	1,020.5	0.0
3	1B	1,361.6	99.0	OO′H′	1,365.2	47.3
4	3A	1,468.8	0.4	O′OH	1,365.2	47.3
5	2B	3,839.7	54.6	OH	3,836.2	34.9
6	4A	3,841.1	14.3	O′H′	3,836.2	34.9
CH_3OH	C_s					
1	1A″	300.4	107.7	$HOCH_i$	348.9	86.8
2	1A′	1,069.6	101.4	CO	1,111.7	114.2
3	2A′	1,100.0	22.0	COH	1,260.4	77.2
4	2A″	1,189.0	0.5	OCH_o	1,302.2	8.6
5	3A′	1,377.8	27.2	OCH_i	1,277.5	2.3
6	4A′	1,485.0	2.6	OCH_o'	1,302.2	8.6
7	3A″	1,505.3	3.5	H_iCH_o	1,487.8	2.7
8	5A′	1,523.2	6.0	H_iCH_o'	1,487.8	2.7
9	6A′	3,019.2	61.6	CH_o	3,044.3	57.4
10	4A″	3,073.3	53.1	CH_o'	3,044.3	57.4
11	7A′	3,134.5	25.3	CH_i	3,120.3	25.0
12	8A′	3,916.3	34.1	OH	3,911.3	33.8
$(H_2O)_2$	C_s					
1	1 A″	129.8	167.2	H3O4H5	264.7	126.3
2	2A″	166.8	3.4	H5O4H3O1	354.7	66.5
3	1A′	168.2	192.3	H3O4H6	264.7	126.3
4	2A′	203.3	106.2	O4H3★	587.6	413.4
5	3A′	381.3	45.0	O1H3O4★	380.9	63.9
6	3A″	643.2	95.4	H2O1H3O4	357.0	98.0
7	4A′	1,637.8	93.4	H5O4H6★	1,621.7	81.0
8	5A′	1,659.2	40.0	H2O1H3★	1,564.4	49.7
9	6A′	3,755.4	330.4	O1H3	3,757.2	390.9
10	7A′	3,871.7	11.1	O4H5	3,902.3	52.8
11	8A′	3,950.4	88.7	O1H2	3,918.1	30.1
12	4A″	3,974.8	85.0	O4H6	3,902.3	52.8

A star indicates that a change in ordering occurred due to an avoided crossing. For a notation of atoms, see Fig. 4

frequencies and two local mode intensities, which in two separate catastrophes (catastrophe points both at $\lambda = \varepsilon$) slit up into five different intensities with weight factors 3:2:1:2:1 (stretching, bending, bending, bending, stretching; see Fig. 1b). In the case of the CH-stretching modes, an intensity value of 22 km/mol associated with the $2T_2$-symmetrical (triply degenerate) asymmetric CH-stretching modes and an intensity of 0 associated with the A_1-symmetrical CH-stretching mode is obtained. It is noteworthy that the intensities of the CH-stretching modes fulfill a sum rule

$$\sum_k^{Nd} (\Delta I)_k = \sum_k^{Nd} (I_{\lambda=\epsilon})_k - (I_{\lambda=0})_k = 0 \tag{46}$$

The *intensity sum rule* is a result of the molecular symmetry and is fulfilled provided that the members of a set of equivalent local modes (i.e., all members of the set have identical local mode frequencies) cannot mix with other modes possessing the same symmetry. Hence, the deviation from the zero value given by the intensity sum rule is a measure for the degree of mode mixing. In Table 3, the sum rule is tested for the infrared intensities of the molecules investigated in this work.

The sum rule of the local mode intensities is nicely fulfilled for the set of local CH-stretching modes (ω_n^a = 3,126 cm^{-1}, Table 2) and the set of local HCH bending modes (ω_n^a = 1,450 cm^{-1}, Table 2). For the former, the positive ΔI values of the three asymmetric CH-stretching intensities ($2T_2$ symmetry) is balanced by the strong decrease in the symmetric CH-stretching intensity ($1A_1$) leading to a sum of just −0.02 km/mol. For the HCH bending intensities, the situation is different as the intensities associated with the $1T_2$- and $1E$-symmetrical mode sets split up into three parts (2:1:2). This is a result of the fact that from six possible HCH bending angles only five are relevant thus fulfilling the requirement $N_{\text{vib}} = N_{\text{para}}$. The sum rule leads to a value of 0.02, which is indicative for some residual mixing of modes of the same symmetry.

In the case of ozone (see Fig. 1c), there is a deviation from the intensity sum rule by 0.67 km/mol (see Table 3), which results from the mixing of the symmetric OO stretching mode with the bending mode. This is stronger

Table 3 Splittings ΔI of intensities of equivalent local modes at the catastrophe point $\varepsilon = 0.01$

Molecule parameter	Sym.	$I_{\lambda=0}$ (km/mol)	$I_{\lambda=\varepsilon}$ (km/mol)	ΔI (km/mol)
H_2O				
OH	$2A_1$	35.49	7.43	−28.06
OH	$1B_2$	35.49	63.52	28.03
Sum				−0.03
CH_4				
HCH	$1T_2$ (×2)	5.43	10.87	5.44
HCH	$1T_2$ (×1)	5.43	3.93	−1.50
HCH	1E (×1)	5.43	1.50	−3.93
HCH	1E (×1)	5.43	0.00	−5.43
Sum				0.02
CH	$1A_1$	15.89	0.00	−15.89
CH	$2T_2$	15.89	21.18	5.29
Sum				−0.02
O_3				
OO	$2A_1$	143.02	0.45	−141.90
OO	$1B_2$	143.02	284.92	142.57
Sum				0.67
HOOH				
OOH	3A	47.31	0.00	−47.31
OOH	1B	47.31	94.67	47.36
Sum				0.05
OH	4A	34.89	14.71	−20.18
OH	2B	34.89	55.07	20.18
Sum				0
CH_3OH				
OCH_o	4A′	8.58	5.53	−3.05
OCH_o	2A″	8.58	10.59	2.01
Sum				−1.04
CH_o	6A′	57.37	53.67	−3.70
CH_o	4A″	57.37	61.11	3.74
Sum				0.04
$(H_2O)_2$				
HOH	1A′	126.29	51.13	−75.16
HOH	1A″	126.29	195.00	68.71
Sum				−6.45
OH	7A′	52.82	19.05	−33.77
OH	4A″	52.82	86.47	33.65
Sum				−0.12

Sum denotes the value according to the sum rule of Eq. (46). For a notation of atoms, see Fig. 4

than in the case of H_2O because of an increase in the bending angle from 105° to 118° (Fig. 4) and a mass ratio equal to 1, which both facilitate mode mixing.

The intensity ACS in Fig. 1c reveals that the intensity of the $1B_2$-symmetrical mode decreases from 284.9 to 231.8 km/mol. This is a direct effect of mass coupling, as reflected by the increase in the negative off-diagonal element of matrix $\mathbf{G}^{-1}$, which connects the asymmetric with the symmetric OO stretching mode. Actually, the same effects can be found for the intensities of the asymmetric XH stretching modes in H_2O and CH_4. However, the decrease in the local mode intensities is much smaller in these cases because mass coupling is smaller for these light–heavy–light situations.

It is interesting to note that the intensity of the local OO stretching modes are high (143 km/mol, Table 2), which is predominantly due to a large ATP element, which in turn is in line with a relatively large change in charge upon OO stretching in a molecule with high biradical character.

For hydrogen peroxide, the sum rule is exactly fulfilled for the OH stretching intensities and approximately for the OOH bending intensities (Table 3). Mass coupling has a relatively small effect on the intensities as can be seen in Fig. 1d. The largest element in the APT is found for the torsional motion as a result of the relatively large change in the charge distribution upon HOOH torsion.

3.3 Methanol, CH_3OH

There are 12 normal and 12 local vibrational modes, which are shown in the frequency ACS of Fig. 2a. The corresponding intensity ACS is given in Fig. 2b. There are familiar features such as the intensity splitting of the two CH_o stretching intensities and that of the two O–C–H_o bending intensities where only the first fulfill the intensity sum rule and the latter deviate because of coupling with other modes of the same symmetry (see Table 3). The CO stretching mode and the H–O–C–H_i torsional mode possess the largest intensities which is due the polarity of the CO bond and the relatively large changes in the charge distribution accompanying these vibrational modes as is confirmed by the corresponding elements of the APT.

Contrary to the intensity ACS shown in Fig. 1a–d, in which the intensity lines mostly change almost linearly (after a possible catastrophe point) from the local mode to the normal mode intensities for $\lambda = 1$, there are strong variations in the intensity of the CO stretching, the C–O–H bending, the O–C–H_o bending, and the O–C–H_i bending modes (Fig. 2b). These variations in the intensity are the results of avoided crossings between these modes. For example, there is an avoided crossing at $\lambda = 0.87$ between modes $1A'$ and $2A'$, which are related to the local CO stretching and C–O–H bending modes (see Fig. 2a). At the avoided crossing, there is a strong mode mixing accompanied by the exchange of mode character and mode energy. Figure 2b reveals that as a consequence also the mode intensities change in the sense that the CO stretching intensity is enhanced and that of the C–O–H bending

intensity by about the same amount decreased. In the region of the avoided crossings, the two intensity curves change in a complementary fashion.

Avoided crossings are also found at $\lambda = 0.02$ between modes $2A'$ and $3A'$, which are related to the local C–O–H and O–C–H_i bending modes (Fig. 2a) and at $\lambda = 0.98$ between modes $4A'$ and $5A'$, which are related to the local O–C–H_o and H–C–H bending modes (Fig. 2a). These avoided crossings are responsible for the steep complementary changes in the C–O–H and O–C–H_i bending intensities I (λ) for small λ (i.e., on the local mode side). Involved is also the local O–C–H_i intensity due to an avoided crossing between modes $3A'$ and $4A'$ (Fig. 2a). The avoided crossing at $\lambda = 0.98$ is however too late to have a large impact on the $4A'$ and $5A'$ intensities (Fig. 2b)

3.4 H_2O dimer, $(H_2O)_2$

The intensity ACS of the water dimer (Fig. 3b) is characterized by a large intensity change of the H-bond (O4 ··· H3) stretching intensity from 588 to 106 km/mol of the $2A'$ mode, which due to a transfer of the mode character from the $3A'$ to the $2A'$ mode at the avoided crossing at $\lambda = 0.8$ (Fig. 3a) where the latter becomes the H-bond stretching mode (mixed with $O1 - H3 \cdots O4$ bending character) and, because of the $2A' - 1A'$ avoided crossing at $\lambda = 0.98$ (Fig. 3a), an addition of H3 ··· O4−H5 bending character [27]. Again at the two avoided crossings, the changes of the $3A'$ and $2A'$ ($2A'$ and $1A'$) intensity curves are complementary (Fig. 3b).

This observation leads to the important conclusion that the local H-bond stretching intensity has a large value because of a large change in charge accompanying the stretching motion. This effects the polarization of the charge distribution in the two water molecules since this is determined by H-bonding. However, mass coupling (caused by stepwise switching on of the masses of the other four atoms in the water dimer; H3 and O4 have already their correct masses) leads to a significant decrease in the intensity. Therefore, the measured normal mode intensity is no longer a reliable descriptor of the charge distribution caused by H-bonding in the dimer.

As noted before, there are no avoided crossings in the intensities. Hence, one must follow the frequency ACS, which is obtained by solving the vibrational eigenvalue problem in dependence of λ to determine that normal mode, which is dominated by H-bond stretching character. This is the $2A'$ mode, which can be confirmed by the analysis of normal modes in terms of local modes [25, 53].

It is noteworthy that the local O1–H3 stretching mode has also a relatively large intensity because it is directly involved in the charge polarization caused by H-bonding. However, this mode ($6A'$) does not experience any avoided crossings with other A' modes (Fig. 3a) and its mass dependence is smaller than that of O4 ··· H3. Therefore, the decrease in the intensity is just from 391 to 330 km/mol (Table 2).

There are also jumps in the intensity ACS curve of the local H3 ··· O4−H5 bending mode (converting to the $1A''$ normal mode, which starts at 126.3 km/mol for $\lambda = 0$ drops down to 51 km/mol because of a catastrophe point (mixing with the H3 ··· O4−H6 bending), then continues to decrease to 0 km/mol because of avoided crossings with the torsional modes H2−O1−H3 ··· O4 and H5−O4 ··· H3−O1 (converting into $3A''$ and $2A''$), and finally experiencing a steep increase to 167 km/mol because of an avoided crossing with the $2A''$ mode at $\lambda = 0.98$, which makes the intensity of the $3A''$ mode drop down to 3 km/mol. Other changes in the intensity curves of Fig. 3b can also be explained by identifying the avoided crossings in the frequency ACS. Conversely, an avoided crossing in the frequency ACS can be confirmed by inspection of the intensity ACS and identifying then the complementary changes in the intensity lines of the modes involved.

4 Chemical relevance of the local mode intensities

As mentioned in the introduction, local mode intensities are derived to get a direct insight into the charge distribution of a molecule. Secondly, the local mode intensities together with the local mode frequencies provide the basis for analyzing infrared spectra. Also, the local mode intensities are tools for a better quantum chemical calculation of infrared intensities. Finally, local mode intensities can be used for the calibration of weakly coupled or completely uncoupled anharmonic oscillator models.

4.1 Infrared intensities and the molecular charge distribution

The derivation of atomic charges from measured quantities has been a major effort in chemistry. Promising in this respect is the determination of effective atomic charges from infrared intensities, [32] which was strongly advocated by Person and Zerbi [33], Galabov and Dudev [34] and their co-workers. The approach had limited success although the line of action was well-defined. This had to do with the fact that for the determination of effective atomic charges, the APT is needed, which could not be obtained from intensities without addition information from quantum chemistry. However, if the APT is fully known, effective atomic charges, which reasonably correlate with

natural bond orbital (NBO) charges, [54] can be determined as was demonstrated by Milani et al. [35].

In our work, we pursue a different approach. We will use the local bond stretching intensities to determine effective bond charges, [34] which determine the charge transfer between two bonded atoms and by this the bond polarity. The exact quantum chemical calculation of the bond polarity is only possible by using highly correlated coupled cluster methods because this requires a well-balanced description of covalent and ionic states in a correlated wave function. For the understanding of bonding, one needs to know the covalent and the ionic (polar) contributions to the bond strength.

The new method of calculating effective bond charges from local mode intensities will comprise the following steps: (i) Calculation of the APT of a target molecule; (ii) Improvement in the APT with the help of measured normal mode intensities; (iii) Use of Eq. (35) to obtain local mode intensities; (iv) Determination of bond charges Δp_n using the relationship $\Delta p_n = \sqrt{I_n^a / G_{nn}}$; and (v) Calculation of bond dipole moments from the known molecular geometry and the Δp_n values. If only relative intensities are measured, which is mostly the case, a reliable quantum chemical calculation of the infrared intensities is needed to convert them into absolute intensities. For quantum chemically calculated intensities, it will be interesting to see how the effective bond polarity and the bond dipole moment derived from local mode intensities differ from those obtained by a population analysis (often derived in a somewhat arbitrary way).

4.2 Analysis of infrared spectra

In this work, we have shown that the normal mode intensities are the result of mode mixing. Therefore, they are not associated with a specific structural unit. By determining the local mode frequency and intensity, the consequences of mode coupling for normal mode frequencies and intensities can be given in detail by the ACS diagrams such as those shown in Figs. 1, 2 and 3. This is particularly interesting when local mode properties are determined on the basis of measured vibrational data [27, 28]. Then, it is possible to determine the strength of a bonding interaction from the local stretching force constant and the bond polarity from the local intensity. Since this information would be extracted from experiment rather than quantum chemical data, the shortcomings of method, basis set, or harmonic approximation used in a quantum chemical calculation would not need to be discussed. Such an analysis would show that H-bonding is combined with a large charge separation contrary to the small intensity of the H-bond stretching band at 143 cm^{-1} [27]. The combination of APT and local mode intensity would provide the effective atomic charges and the magnitude of the effective bond charge equal to the charge transfer.

4.3 Improved scaling procedures

The local mode frequencies can be used for a superior scaling of quantum chemical frequencies calculated for large molecules utilizing the harmonic approximation. Since a local mode is associated with a given internal coordinates, local mode frequencies for molecular units such as XH, AB, ABH, ABC, etc. can be determined from measured [26] and calculated frequencies. The determination of scaling factors for well-defined structural units is straightforward and can be used to an individual normal mode frequency. Each normal mode can be decomposed into local mode contributions, i.e., for each mode the percentage of XH stretching, ABC bending, etc. can be determined. Then, each mode contribution is assigned the appropriate local mode scaling factor and an individual frequency scaling factor is calculated from the properly weighted local scaling factors of the local modes contributing to the normal mode in question. This dynamic scaling approach is superior to previous static scaling procedures, which could not consider the effect of mode coupling. A stretching mode may have a significant contribution from bending, and therefore, significant down-scaling of the frequency as needed for pure stretching frequencies is inappropriate because harmonic bending frequencies have to be less reduced than harmonic stretching frequencies.

The need for individual intensity scaling is even larger than for frequency scaling as was emphasized in various articles [55, 56]. The use of an individual scaling scheme as described in the case of the normal mode frequencies is only possible with the help of the local mode intensities. For example, in a recent investigation, the cyano-stretching intensities were scaled with a common factor leading to an improved but not exact agreement with experiment [56]. This we see as a result of different coupling situations for the CN stretching vibration with other modes, thus triggering stronger changes in the intensity ACS. Another source of error results from solvent influences, which are different for polar and nonpolar groups in a molecule. The calculation of local mode intensities can provide exact information with regard to solvent dependable intensity changes.

4.4 Calibration of harmonically coupled oscillator models (HOM)

The local mode model of molecular vibrations developed in the 70s by Henry et al. [37] has been used in the description of CH-stretching overtone spectra [38–40, 57,

58]. In this approach, harmonically coupled Morse oscillators (including anharmonicity effects) are used to quantum mechanically determine the vibrational frequencies and wave functions of the HOM. By employing quantum chemical methods to calculate the dipole moment function and then the oscillator strengths in the CH-stretching overtone spectra of various small and medium-seized organic molecules (alkanes, alkenes, alcohols, H-bonded complexes, etc.) a useful account of frequencies and intensities of overtones up to $v = 6$ could be determined [23].

In previous work, Cremer and co-workers demonstrated that the local mode frequencies of Konkoli and Cremer [24] linearly correlate ($R^2 = 0.990$) with the overtone frequencies of Henry for $v = 6$ [11]. Also, it could be shown by these authors that residual couplings lead to deviations from the ideal local oscillator model. This opens up the possibility of providing suitable local force constants for the parametrization of the HOM. This can be done for anharmonically corrected force constants where the latter are derived from measured vibrational frequencies using the Konkoli–Cremer approach [26]. Rong et al. [40] observed that the harmonically coupled anharmonic oscillator model leads to exaggerated intensities depending on the quantum chemical method and basis set used for calculating the dipole moment function. Clearly, the prediction of overtone intensities can be improved by proper scaling where again local mode intensities derived from experiment and from calculations would lead to suitable scaling factors as described in the previous subsection.

5 Conclusions

In this work, we have introduced the local mode intensities and the intensity ACS for the purpose of analyzing normal mode intensities. A number of conclusions can be drawn from the work presented here.

1. The local mode intensity has been derived by expressing the normal mode intensity in internal coordinates and then applying the adiabatic condition ($\lambda = 0$), which leads to three requirements defining $\mathbf{D}_0, \mathbf{M}_0^R, \tilde{\mathbf{D}}_0$, and by this also the local mode intensity I_n^a associated with mode $\mathbf{a}_n$ and the internal coordinate q_n. Local mode intensities I_μ^{nm} are independent of the coordinates q_m, $(m \neq n)$ used for the description of the molecular geometry. They are also independent of any variation in the isotope distribution in other parts of the molecule but the target fragment described by q_n. The local mode intensity values of a molecule comply with the molecular symmetry and become identical for diatomic molecules to the normal mode intensity.
2. The intensity ACS has been derived in this work by exploiting the dependence of the normalized internal coordinate mode vectors on λ, which can be expressed in the form $(\mathbf{G}_\lambda)^{-1}\tilde{\mathbf{D}}_\lambda$. The first term of the matrix product reflects the effect of mass coupling on the intensity, which increases as the off-diagonal elements of the **G**-matrix increase with λ. The second product term describes the effect of mode mixing on the intensity I_λ.
3. Mass coupling leads to an essentially linear decrease or increase in the local to the normal mode intensity. This can be anticipated by an analysis of the matrix $\mathbf{G}^{-1}$.
4. Symmetry-equivalent local modes strongly couple, which leads to a large change in the corresponding intensities upon an infinitesimal increase of λ from 0 to ϵ, for which we have coined the term *intensity catastrophe* because the sudden change in the local mode intensities complies with the mathematical definition of a catastrophe [51]. The changes in the intensities accompanying an intensity catastrophe depend on the position of the local mode units in the molecule (proximity effect), the alignment of the local mode vectors, the ratio of the masses involved and the change in the charge distribution caused by the local mode vibrations.
5. All members of a group of equivalent local modes are involved in an intensity catastrophe and if there is no coupling with modes outside the group, the intensity changes ΔI caused by the catastrophe sum to zero (*intensity sum rule*). The deviation from the sum rule is a quantitative measure for the coupling with other modes of the same symmetry.
6. Avoided crossings in the frequency ACS between modes of the same symmetry can lead to strong nonlinear changes in the intensity curves I_λ, which are largely complementary for the vibrational modes involved. Depending on the type of avoided crossing, the mode character is transferred from one mode to the other or the original mode changes its character by absorbing additional local mode contributions. This has to be considered when analyzing intensity changes from local to normal modes.
7. There are no avoided crossings in an intensity ACS. However avoided crossings in the frequency ACS can be detected by identifying modes with strong, but complementary changes in the intensities.
8. In each case investigated, one obtains detailed physical explanations why a normal mode intensity adopts a particular value. This is facilitated by evaluating matrices $\mathbf{\Lambda}, \mathbf{M}^{-1}, \mathbf{B}^\dagger, (\mathbf{G}_\lambda)^{-1}$, and $\tilde{\mathbf{D}}_\lambda$ for

specific values of λ between 0 and 1 where the first three matrices do not change with λ.

9. There have been attempts to relate normal mode intensities to bond charges [34, 47]. On the background of this work, we can say that these attempts are only meaningful in cases of minimal local mode coupling and large mass ratios. In general, this approach is useless as long as it does not start from local mode intensities.
10. We have shown the chemical relevance of local mode intensities with regard to the determination of bond charges and bond polarity, for the analysis of infrared spectra, for the development of a dynamic scaling method of calculated harmonic infrared intensities, and for the calibration of harmonic and anharmonic oscillator models.

In this work, we have not put emphases on the correct calculation of the infrared intensities because the derivation of the basic concept of local mode intensities and the analysis of normal mode intensities in terms of the former is at the primary focus of this work. However, in future work we will focus on the determination of local mode intensities from experimental intensities or coupled cluster intensities. Also, we will derive effective bond charges from local mode intensities, which are no longer contaminated by mass- or mode-coupling.

Acknowledgments This work was financially supported by the National Science Foundation, Grant CHE 1152357. We thank SMU for providing computational resources.

References

1. Pauling L (1960) The nature of the chemical bond. Cornell University Press, Ithaca
2. Lide DR (2009) CRC handbook of chemistry and physics, 90th edn. CRC, Boca Raton, FL
3. Luo Y-R (2007) Comprehensive handbook of chemical bond energies. Taylor and Francis, Boca Raton
4. Herzberg G, Huber KP (1979) Spectra and molecular structure. IV. Constants of diatomic molecules. Van Nostrand, Reinhold, NY
5. Cremer D, Wu A, Larsson A, Kraka E (2000) Some thoughts about bond energies, bond lengths, and force constants. J Mol Model 6:396–412
6. Kalescky R, Kraka E, Cremer D (2013) Identification of the strongest bonds in chemistry. J Phys Chem A 117:8981–8995
7. Cremer D, Kraka E (2010) From molecular vibrations to bonding, chemical reactions, and reaction mechanism. Curr Org Chem 14:1524–1560
8. Wilson EB, Decius JC, Cross PC (1955) Molecular vibrations. The theory of infrared and Raman vibrational spectra. McGraw-Hill, New York
9. Woodward LA (1972) Introduction to the theory of molecular vibrations and vibrational spectroscopy. Oxford University Press, Oxford
10. Badger RM (1934) A relation between internuclear distances and bond force constants. J Chem Phys 2:128–131
11. Kraka E, Larsson A, Cremer D (2010) Generalization of the badger rule based on the use of adiabatic vibrational modes in vibrational modes in computational IR spectroscopy. In: Grunenberg J (ed) Computational spectroscopy: methods, experiments and applications, Wiley, New York, p 105
12. Silverstein RM, Webster FX, Kiemle D (2005) Spectrometric identification of organic compounds. Wiley, Hobroken
13. Smith B (1999) Infrared spectral interpretation: a systematic approach. CRC Press, Boca Raton
14. Decius JC (1963) Compliance matrix and molecular vibrations. J Chem Phys 38:241–248
15. Grunenberg J, Goldberg N (2000) How strong is the Gallium≡Gallium triple bond? Theoretical compliance matrices as a probe for intrinsic bond strengths. J Am Chem Soc 122:6045–6047
16. Brandhorst K, Grunenberg J (2008) How strong is it? The interpretation of force and compliance constants as bond strength descriptors. Chem Soc Rev 37(8):1558–1567
17. Brandhorst K, Grunenberg J (2010) Efficient computation of compliance matrices in redundant internal coordinates from Cartesian Hessians for nonstationary points. J Chem Phys 132:184101–184107
18. Madhav MV, Manogaran S (2009) A relook at the compliance constants in redundant internal coordinates and some new insights. J Chem Phys 131:174112–174116
19. Espinosa A, Streubel R (2011) Computational studies on azaphosphiridines, or how to effect ring-opening processes through selective bond activation. Chem Eur J 17:3166–3178
20. McKean DC (1978) Individual CH bond strengths in simple organic compounds: effects of conformation and substitution. Chem Soc Rev 7:399–422
21. Duncan JL, Harvie JL, McKean DC, Cradock C (1986) The ground-state structures of disilane, methyl silane and the silyl halides, and an SiH bond length correlation with stretching frequency. J Mol Struct 145:225–242
22. Murphy WF, Zerbetto F, Duncan JL, McKean DC (1993) Vibrational-spectrum and harmonic force-field of trimethylamine. J Phys Chem 97:581–595
23. Henry BR (1987) The local mode and overtone spectra: a probe of molecular structure and conformation. Acc Chem Res 20:429–435
24. Konkoli Z, Cremer D (1998) A new way of analyzing vibrational spectra. I. Derivation of adiabatic internal modes. Int J Quantum Chem 67:1–9
25. Konkoli Z, Cremer D (1998) A new way of analyzing vibrational spectra. II. Characterization of normal vibrational modes in terms of internal vibrational modes. Int J Quantum Chem 67:29–40
26. Cremer D, Larsson JA, Kraka E (1998) New developments in the analysis of vibrational spectra: on the use of adiabatic internal, vibrational modes. In: Parkanyi C (ed) Theoretical and computational chemistry, volume 5, theoretical organic chemistry. Elsevier, Amsterdam, p 259
27. Kalescky R, Zou W, Kraka E, Cremer D (2012) Local vibrational modes of the water dimer—comparison of theory and experiment. Chem Phys Lett 554:243–247
28. Kalescky R, Kraka E, Cremer D (2013) Local vibrational modes of the formic acid dimer—the strength of the double hydrogen bond. Mol Phys 111:1497–1510
29. Larsson A, Cremer D (1999) Theoretical verification and extension of the McKean relationship between bond lengths and stretching frequencies. J Mol Struct 485:385–407
30. Zou W, Kalescky R, Kraka E, Cremer D (2012) Relating normal vibrational modes: to local vibrational modes with the help of an adiabatic connection scheme. J ChemPhys 137:084114
31. Zou W, Kalescky R, Kraka E, Cremer D (2012) Relating normal vibrational modes to local vibrational modes: benzene and naphthalene. J Mol Model 19:2865–2877
32. Person WB, Newton JH (1974) Dipole moment derivatives and infrared intensities. I. Polar tensors. J Chem Phys 61:1040–1049

33. Person WB, Zerbi G (1982) Vibrational Intensities in infrared and Raman spectroscopy. Elsevier, Amsterdam
34. Galabov B, Dudev T (1996) Vibrational intensities. Elsevier, Amsterdam
35. Milani A, Tommasini M, Castiglioni C (2012) Atomic charges from ir intensity parameters: theory, implementation and application. Theor Chem Acc 131:1–17
36. Boatz JA, Gordon MS (1989) Decomposition of normal-coordinate vibrational frequencies. J Phys Chem 93:1819, 1989
37. Hayward RJ, Henry BR (1975) A general local-mode theory for high energy polyatomic overtone spectra and application to dichloromethane. J Mol Spectrosc 57:221–235
38. Kjaergaard HG, Yu H, Schattka BJ, Henry BR, Tarr AW (1990) Intensities in local mode overtone spectra: propane. J Chem Phys 93:6239–6248
39. Kjaergaard HG, Turnbull DM, Henry BR (1993) Intensities of CH- and CD-stretching overtones in 1,3-butadiene and 1,3-butadiene-d_6. J Chem Phys 99:9438–9452
40. Rong Z, Henry BR, Robinson TW, Kjaergaard HG (2005) Absolute intensities of CH stretching overtones in alkenes. J Phys Chem A 109:1033–1041
41. Jacob CR, Luber S, Reiher M (2009) Understanding the signatures of secondary-structure elements in proteins via Raman optical activity spectroscopy. Chem Eur J 15:13491–13508
42. Jacob CR, Reiher M (2009) Localizing normal modes in large molecules. J Chem Phys 130:084106
43. Liegeois V, Jacob CR, Champagne B, Reiher M (2010) Analysis of vibrational Raman optical activity signatures of the $(TG)_N$ and $(GG)_N$ conformations of isotactic polypropylene chains in terms of localized modes. J Phys Chem A 114:7198–7212
44. Sokolov VI, Grudzev NB, Farina IA (2003) Local vibrational mode in zinc telluride associated with a charged nickel impurity. Phys. Solid State 45:1638–1643
45. Sangster MJL, Harding JH (1986) Calculation of local and gab mode frequencies from impurities in alkali halide crystals. J Phys C Solid State Phys 19:6153–6158
46. Califano S (1976) Vibrational states. Wiley, London
47. Zerbi G (1982) Introduction to the theory of vibrational frequencies and vibrational intensities. In: Person W and Zerbi G (eds) Vibrational intensities in infrared and Raman spectroscopy, Elsevier, Amsterdam, p 23
48. Yamaguchi Y, Goddard JD, Osamura Y, Schaefer HFS (1994) A new dimension to quantum chemistry: analytic derivative methods in ab initio molecular electronic structure theory. Oxford University Press, Oxford
49. Chai J-D, Head-Gordon M (2008) Long-range corrected hybrid density functionals with damped atomatom dispersion corrections. Phys Chem Chem Phys 10:6615–6620
50. Dunning TH (1989) Gaussian basis sets for use in correlated molecular calculations. J Chem Phys 90:1007–1023
51. Thom R (1975) Structural stability and morphogenesis. Benjamin, Reading
52. Poston T, Stewart I (1981) Catastrophe theory and its applications. Pitma, Boston
53. Konkoli Z, Larsson JA, Cremer D (1998) A new way of analyzing vibrational spectra IV. Application and testing of adiabatic modes within the concept of the characterization of normal modess. Int J Quantum Chem 67:41
54. Reed AE, Curtiss LA, Weinhold F (1988) Intermolecular interactions from a natural bond orbital, donor–acceptor viewpoint. Chem Rev 88:899
55. Hallas MD, Schlegel HB (1998) Comparison of the performance of local, gradient-corrected, and hybrid density functional models in predicting infrared intensities. J Chem Phys 109:10587–10593
56. Stoyanov SS (2010) Scaling of computed cyano-stretching frequencies and IR intensities of nitriles, their anions, and radicals. J Phys Chem A 114:5149–5161
57. John U, Nair KPR (2005) Near ir overtone spectral investigations of cyclohexanol using local mode model-evidence for variation of anharmonicity with concentration due to hydrogen bonding. Spectrochim Acta A 61:2555–2559
58. Morita M, Takahashi K (2013) Multidimensional oh local mode calculations for $OH^-(H_2O)_3$-importance of intermode anharmonicity. Phys Chem Chem Phys 15:114–124